Steady states and global dynamics of electrical activity in the cerebral cortex

P. A. Robinson,[1,*] C. J. Rennie,[1,2,†] J. J. Wright,[3,‡] and P. D. Bourke[3,§]
[1]*School of Physics, University of Sydney, Sydney, New South Wales 2006, Australia*
[2]*Department of Medical Physics and Cognitive Neuroscience Unit, Westmead Hospital, Westmead, New South Wales 2145, Australia*
[3]*Mental Health Research Institute, Parkville, Victoria 3052, Australia*
(Received 6 March 1998)

Steady states and global dynamics of electrical activity in the cerebral cortex are investigated within the framework of a recent continuum model. It is shown that for a particular physiologically realistic class of models, at most three steady states can occur, two of which are stable. The global dynamics of spatially uniform activity states is studied and it is shown that in a physiologically realistic class of models, the adiabatic dynamics is governed by a second-order differential equation equivalent to that for the motion of a Newtonian particle in a potential in the presence of friction. This result is used to derive a simplified dynamical equation in the friction-dominated limit. Solutions of these equations are compared with those of the full global dynamics equations and it is found that they are adequate for time scales longer than approximately 100 ms provided dendritic integration times are less than approximately 10 ms. [S1063-651X(98)12908-2]

PACS number(s): 87.22.Jb, 87.22.As, 87.10.+e

I. INTRODUCTION

Recently we developed a continuum model for the propagation of electrical activity in the cerebral cortex [1]. This model traced the evolution of quantities such as the neuronal firing rate, averaged over volumes large enough to contain many neurons, as in several previous works [2–12]. Both excitatory and inhibitory neuronal populations were included, as were the effects of nonlinear neural responses, temporal integration in the dendrites, and propagation time delays in the axons. This model allowed us to write down equations for dynamics, steady state solutions, and dispersion and stability of linear waves.

The above model did not include the effects of feedback on the basic parameters of the cortex, such as the threshold potential for neuronal firing, and the effective strengths of coupling between various neuronal populations. Such feedbacks are known to be of central importance in the dynamics of the actual cortex: The state of arousal (e.g., relaxed vs alert) strongly affects the cortical response to stimuli as measured by electroencephalograms (EEGs), for example [13]. Such responses are normally termed *evoked response potentials*. These responses depend not only upon fast cortical responses on time scales well below 100 ms (e.g., voltage-dependent changes in ion conductivities of neuronal membranes), but on feedbacks that evolve over longer intervals (e.g., the action of chemical neurotransmitters) [14]. In general, we take feedbacks to include any modulation of cortical parameters that depends on the cortical state and/or its history.

Another area in which feedbacks are of importance is in the onset and termination of seizures. It is likely that the cortex operates in a state close to marginal stability [1] so as to be stable, but not so stable that all interesting behavior is suppressed. Normal subjects are not prone to spontaneous seizures, whereas in epilepsy, for example, the cortex can undergo a transition to a seizure state in which all the neurons are firing far above their normal rate. Such seizures are not permanent: Some feedback mechanism (or combination of mechanisms) acts to return the brain to its normal state after seconds or minutes [7,13].

The purpose of the present work is to understand better the steady states and global dynamics of a generalized version of the model introduced in our previous work [1], an essential step prior to incorporating feedbacks in future works. In Sec. II we study the possible steady-state solutions of the generalized model, deriving a steady-state equation and limits on the maximum number of steady states in certain cases. Apart from being the simplest and most fundamental solutions of the model, these steady states and their basins of attraction determine the qualitative dynamics in the absence of feedback and provide strong constraints on the dynamics more generally for slow feedbacks. In Sec. III we study how the steady states and their interrelationships depend on the underlying parameters of the model, demonstrating that a class of models that is particularly plausible physiologically has simple properties in this respect, possessing only three steady states.

Many observations of electrical activity in the cortex are made at relatively coarse spatial scales. EEGs, for example, often use scalp electrodes separated by several centimeters, while most short-scale features are filtered out as a result of the conductivity of the cerebrospinal fluid, skull, and scalp in any case [7]. In addition, Robinson *et al.* [1] showed that the longest-wavelength eigenstates are the least damped and thus are likely to contain the most spectral power when the cortex is driven by noise or complex inputs. Hence, in Sec. IV we study the large-scale dynamics of the cortex. Furthermore, we do this in a simplified way by specializing to adiabatic dynamics, which we define to be dynamics on time scales much larger than the dendritic integration time of order 5–10 ms [1,5]. We show that the spatially uniform global dynam-

*Electronic address: robinson@physics.usyd.edu.au
†Electronic address: rennie@physics.usyd.edu.au
‡Electronic address: jjw@mhri.edu.au
§Electronic address: pdb@mhri.edu.au

ics of the cortex can be described by an equation that is equivalent to that of a Newtonian particle moving under the influence of friction in a potential whose minimums define the stable steady states of the system. When friction dominates it is also possible to write down a simplified first-order equation for the adiabatic dynamics in the governing potential. Numerical results show that these adiabatic equations approximate the dynamics well for time scales exceeding ~ 100 ms. In future work, extension of these equations to incorporate adiabatic feedback will enable the qualitative dynamical effects of various types of feedback to be determined by looking at their effects on the potential and the resulting ''forces'' on the system. This ability is relevant to any analysis of feedback processes that adiabatically modify the basins of attraction of the steady-state solutions of the dynamical equations. Faster feedback mechanisms also interact with the basins of attraction, but an adiabatic approximation is not possible.

It should be stressed that real cortical electrical activity involves spatially nonuniform eigenmodes, as well as the spatially uniform ones studied here. Inclusion of these modes, and the corresponding nonlinear mode-mode interactions, along with feedback, will also be essential in any full understanding of cortical waves and EEGs.

II. STEADY STATES OF THE CEREBRAL CORTEX

In this section we categorize the steady-state solutions of our dynamical model of the cortex [1]. In Sec. II A we briefly review the dynamical equations themselves. Section II B generalizes our earlier fixed-point analysis [1] and derives a single fixed-point equation whose solutions determine the steady states. Section II C discusses the fixed points in general and in some special cases where their numbers are strictly limited. Finally, necessary conditions for the occurrence of multiple stable steady states are derived in Sec. II D. The mathematical analysis presented in the latter parts of this section is essential to the understanding of the physical behaviors studied in Secs. III and IV.

A. Dynamical equations

In this section we first outline the main relevant results of our recently developed wave-equation formulation of continuum cortical dynamics [1]. In a previous paper [1] we developed a set of nonlinear equations for cortical dynamics in the continuum limit. These equations incorporated excitatory and inhibitory neurons, dendritic integration of inputs to a given neuron, finite axonal propagation velocities, and the nonlinear relationship between inputs to a neuron and its firing rate. In all cases, the dynamical quantities are assumed to be averaged over a volume large enough to contain many neurons but very small relative to the whole cortex. This continuum approximation is easy to justify as there are $\sim 10^{10}$ neurons in the cortex. Other continuum analyses have been carried out previously [2–12], with some authors obtaining linear or nonlinear wave equations as a result [6,7,11,12], but we restrict attention here to the analysis of a generalization of our previous model [1].

The first of the central equations of our model is

$$Q_{e,i}=\sigma(V_{e,i}), \tag{1}$$

which relates the mean firing rates Q_e and Q_i of neurons (the *pulse densities* in neurophysiological terminology) to the applied potentials V_e and V_i, where e and i denote the excitatory and inhibitory populations. The function $\sigma(x)$ represents the fraction of neurons that will fire at or below an incident potential x; we assume that it is the same monotonically increasing function for both neuronal populations, with the properties

$$\lim_{x\to-\infty}\sigma(x)=0, \tag{2}$$

$$\lim_{x\to\infty}\sigma(x)=1. \tag{3}$$

In general, σ can be written in the form

$$\sigma(x)=\int_{-\infty}^{x}\sigma'(u)du, \tag{4}$$

where $\sigma'(u)$ is a non-negative, singly peaked, integrable, bell-shaped function, which we will assume to be symmetric about its peak. We also assume that the first few derivatives of σ and its inverse are continuous. If we work in $V_{e,i}$ units in which the full width at half maximum of σ is of order unity, we can conclude that the maximum of $d\sigma(V_{e,i})/dV_{e,i}$ is also of order unity, since Eqs. (3) and (4) must be satisfied. Figure 1 shows an example of σ and its first three derivatives [the specific form used is the one employed in Secs. III and IV, defined by Eq. (33) below].

The quantity $V_{e,i}$ is defined to be the neuronal potential at the cell body where conversion to neuronal pulses takes place after inputs have been summed and filtered through the dendrites. A good approximation to $V_{e,i}$ is given by [1]

$$V_{e,i}=g_{e,i}\frac{\alpha\beta}{\beta-\alpha}[U_{e,i}-W_{e,i}], \tag{5}$$

$$\frac{dU_{e,i}}{dt}=Q_{ae,ai}-\alpha U_{e,i}, \tag{6}$$

$$\frac{dW_{e,i}}{dt}=Q_{ae,ai}-\beta W_{e,i}, \tag{7}$$

where $Q_{ae,ai}$ represent mean arrival rates of input pulses at the dendrites, $g_{e,i}$ are dendritic gain factors, and α and β are constants parametrizing the dendritic response to an impulse. In effect dendritic propagation smears out the temporal response over a time scale $\sim\max\{\alpha^{-1},\beta^{-1}\}$ and the dendritic tree acts as a low-pass filter. Equation (5) generalizes our previous corresponding equation [1] by allowing g_e and g_i to differ.

Outgoing pulses from each neuron propagate along its axon and axonal tree at a characteristic velocity v. Assuming an isotropic distribution of axons with approximately exponentially distributed ranges (see Ref. [1] for the exact distribution), this propagation can be modeled by a wave equation for the corresponding potentials $\phi_{e,i}$:

$$\left(\frac{\partial^2}{\partial t^2}+2\gamma_{e,i}\frac{\partial}{\partial t}+\gamma_{e,i}^2-v^2\nabla^2\right)\phi_{e,i}=\gamma_{e,i}^2Q_{e,i}, \tag{8}$$

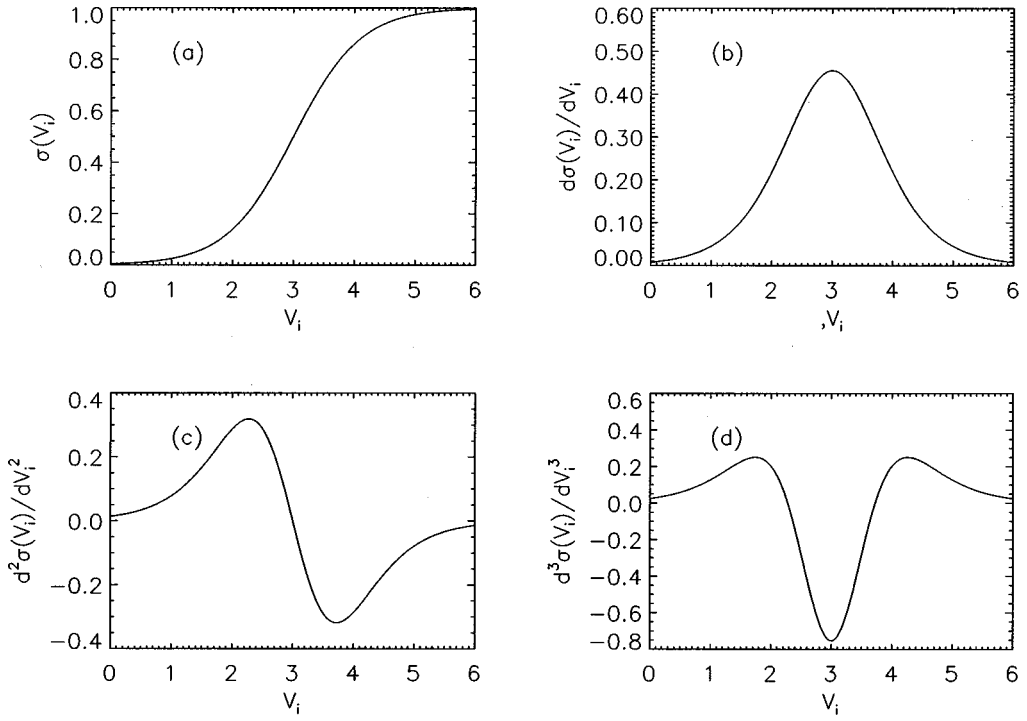

FIG. 1. Example of the function $\sigma(V_i)$ and its derivatives with respect to V_i, as calculated from Eqs. (33) and (A1)–(A3): (a) $\sigma(V_i)$, (b) first derivative, (c) second derivative, and (d) third derivative.

where $\gamma_{e,i}=v/r_{e,i}$ and $r_{e,i}$ are the characteristic ranges of the axons [1].

The incident potentials $Q_{ae,ai}$ at a particular location comprise contributions from the wave potentials $\phi_{e,i}$ and inputs ϕ_s from outside the cortex. This leads to the final underlying equations of our model:

$$Q_{ae}=a_{es}\phi_s+a_{ee}\phi_e-a_{ei}\phi_i, \tag{9}$$

$$Q_{ai}=a_{is}\phi_s+a_{ie}\phi_e-a_{ii}\phi_i. \tag{10}$$

Here the constants a_{mn} are the fractional synaptic densities associated with excitatory, inhibitory, and subcortical inputs $\phi_{e,i,s}$ to excitatory and inhibitory neurons. A change of notation from some of our previous work [1,15] is that ϕ_s now represents all external inputs to the cortex, thereby combining the quantities Q_s and Q_{ns} used previously [1,8–10] to denote time-varying and static inputs, respectively. The coefficients $a_{es,is}$ also subsume the four coefficients $M_{e,i}$ and $\mu_{e,i}$ that previously parametrized the contributions of time-varying and static inputs. Normalizations of the a_{mn} are discussed in Sec. III B.

B. Steady state equation

If we set all the time derivatives in Eqs. (6)–(8) equal to zero and, furthermore, seek spatially uniform solutions of these equations, we find

$$V_{e,i}=g_{e,i}Q_{ae,ai}, \tag{11}$$

$$\phi_{e,i}=Q_{e,i}, \tag{12}$$

with Eqs. (1), (9), and (10) unchanged, except that ϕ_s is now understood to be the time- and space-independent component of ϕ_s. Equations (1) and (9)–(12) now yield

$$V_e=b_{es}\phi_s+b_{ee}\sigma(V_e)-b_{ei}\sigma(V_i), \tag{13}$$

$$V_i=b_{is}\phi_s+b_{ie}\sigma(V_e)-b_{ii}\sigma(V_i) \tag{14}$$

after eliminating $\phi_{e,i}$, $Q_{e,i}$, and $Q_{ae,ai}$, and writing $b_{mn}=g_m a_{mn}(\geqslant 0)$ for compactness. Equation (14) implies

$$V_e=\sigma^{-1}(y), \tag{15}$$

$$y=\frac{1}{b_{ie}}[V_i+b_{ii}\sigma(V_i)-b_{is}\phi_s] \tag{16}$$

$(y=Q_e)$. This solution is unique because we find that the right-hand side of Eq. (16) is monotonically increasing with V_i. Hence there is a unique value of $\sigma(V_e)$ for any value of V_i. The function $\sigma(V_e)=y$ is also monotonically increasing with V_e (i.e., it is one to one), so there is a unique inverse V_e in Eq. (15).

If we substitute Eq. (15) into Eq. (13) we find that the steady-state values of y are given by the roots of $f(y)$, with

$$f(y)=\sigma^{-1}(y)-b_{ee}y+b_{ei}\sigma(V_i)-b_{es}\phi_s. \tag{17}$$

Steady state values of other variables then follow from the application of Eqs. (1), (9)–(12), and (15). The following subsections are concerned with the properties of Eq. (17) and its roots.

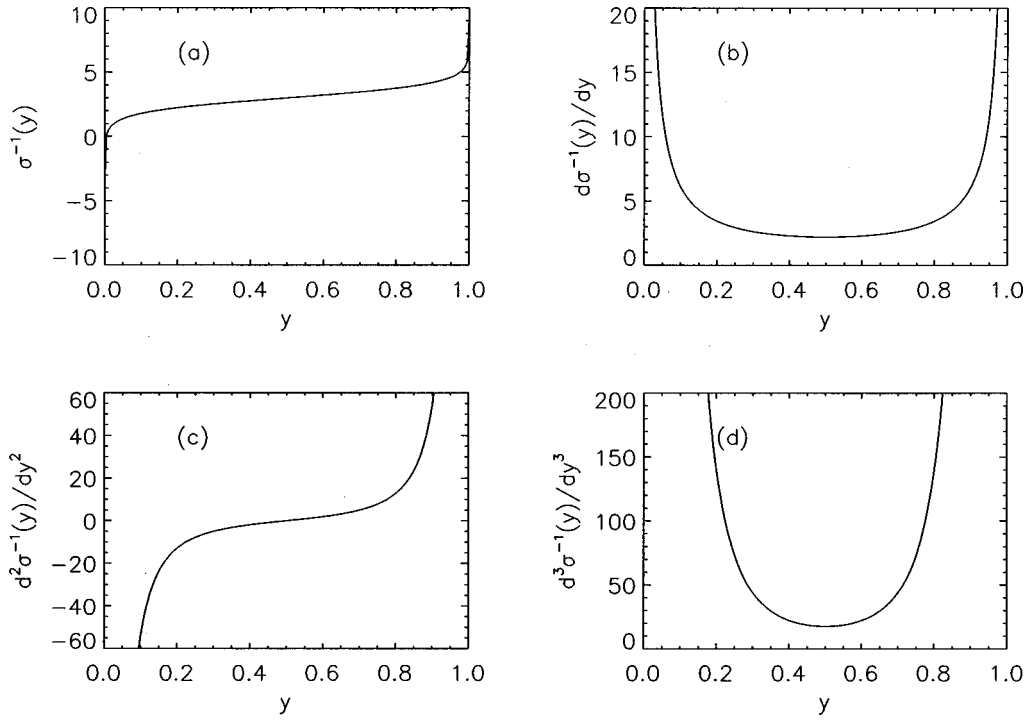

FIG. 2. Example of the function $\sigma^{-1}(y)$ and its derivatives with respect to y, as calculated from Eqs. (34) and (A4)–(A6): (a) $\sigma^{-1}(y)$, (b) first derivative, (c) second derivative, and (d) third derivative.

C. Number of steady states

Looking at Eq. (17), we note that y and $\sigma(V_i)$ are bounded on the interval (0,1), whereas $\sigma^{-1}(y)$ is unbounded (see Fig. 2), with

$$\lim_{y\to 1^-} \sigma^{-1}(y)=\infty, \tag{18}$$

$$\lim_{y\to 0^+} \sigma^{-1}(y)=-\infty. \tag{19}$$

(Of course, $\sigma^{-1}(y)$ is undefined outside the open interval (0,1).) Hence $f(y)$ runs from $-\infty$ to ∞ as y runs from 0 to 1. Since $f(y)$ is real and continuous, this implies that there is at least one root and, in general, an odd number of roots, each corresponding to a cortical steady state.

If f has N zeros and is continuous and differentiable, then df/dy must have at least $N-1$ zeros. If we can show that df/dy has no zeros, then f must have *exactly* one. If we can show df/dy has at most 2, 4, etc. zeros, then f must have at most 3, 5, etc. zeros, respectively.

We can use Eq. (16) to eliminate $\sigma(V_i)$ from Eq. (17), giving

$$f(y)=\sigma^{-1}(y)+Ay-BV_i+C\phi_s, \tag{20}$$

$$A=\frac{b_{ei}b_{ie}}{b_{ii}}-b_{ee}, \tag{21}$$

$$B=b_{ei}/b_{ii}, \tag{22}$$

$$C=\frac{b_{ei}b_{is}}{b_{ii}}-b_{es}. \tag{23}$$

We then find

$$\frac{df}{dy}=\frac{d\sigma^{-1}(y)}{dy}+A-B\frac{dV_i}{dy} \tag{24}$$

$$=\frac{d\sigma^{-1}(y)}{dy}+A-\frac{Bb_{ie}}{1+b_{ii}\dfrac{d\sigma(V_i)}{dV_i}}. \tag{25}$$

Some general properties of f and its derivative are that (i) $B>0$, whereas A and C can have either sign; (ii) $d\sigma^{-1}(y)/dy$ is symmetric about $y=1/2$ (see Fig. 2), with

$$\lim_{y\to 0^+}\frac{d\sigma^{-1}(y)}{dy}=\lim_{y\to 1^-}\frac{d\sigma^{-1}(y)}{dy}=\infty, \tag{26}$$

because of the properties of $\sigma(y)$ discussed in Sec. II A; (iii)

$$\frac{d\sigma^{-1}(y)}{dy}>0 \tag{27}$$

for all y; and (iv) the denominator of the term involving B in Eq. (25) is always $\geqslant 1$ because $\sigma(V_i)$ is monotonically increasing with V_i (see Fig. 1), i.e.,

$$\frac{d\sigma(V_i)}{dV_i}>0. \tag{28}$$

We now use the above results to determine the maximum number of roots of $f(y)$ in some special cases. If $b_{ei}b_{ie}=0$ and the other b_{mn} are arbitrary, Eq. (25) implies

$$\frac{df(y)}{dy}=\frac{d\sigma^{-1}(y)}{dy}-b_{ee}. \tag{29}$$

Equation (29) has either zero or two roots since the first term on the right-hand side is strictly positive and has only a single minimum (at $y=\frac{1}{2}$), while the second is constant. Hence $f(y)$ has at most three roots.

Equation (17) yields

$$\frac{df(y)}{dy}=\frac{d\sigma^{-1}(y)}{dy}+b_{ei}\frac{d\sigma(V_i)}{dy}-b_{ee}. \tag{30}$$

The first two terms in this equation are strictly positive, so it has no roots if b_{ee} satisfies

$$b_{ee}<\left.\frac{d\sigma^{-1}(y)}{dy}\right|_{\min}=O(1), \tag{31}$$

with the other b_{mn} arbitrary. In this case, $f(y)$ has exactly one root. This can also be seen by noting that the sum of the first two terms in Eq. (17) is monotonically increasing in this case, as is the third term; hence Eq. (17) has just one root.

D. Conditions for the occurrence of various numbers of steady states

Here we list several necessary or sufficient conditions for the occurrence of one, three, or five or more roots. We will apply these conditions to a specific version of σ in Sec. III.

1. Sufficient condition for exactly one root

A sufficient condition for there to be exactly one root is that $f(y)$ be monotonically increasing. This is certainly the case when b_{ee} satisfies Eq. (31).

2. Conditions for three or more roots

A necessary condition for there to be at least three roots is that $df(y)/dy$ be negative for some y and hence that this quantity change sign at some point. Differentiation of Eq. (17) yields

$$\frac{df(y)}{dy}=\frac{d\sigma^{-1}(y)}{dy}-b_{ee}+\frac{b_{ie}b_{ei}\sigma'(V_i)}{1+b_{ii}\sigma'(V_i)}, \tag{32}$$

where primes denote differentiation with respect to V_i. The first and last terms in Eq. (32) are non-negative, so a necessary condition for $f(y)$ to change sign is Eq. (31) with the inequality reversed, since the final term in Eq. (32) approaches zero at large $|V_i|$.

The function $f(y)$ is bounded above and below by the functions obtained by replacing $\sigma(V_i)$ in Eq. (17) by 1 and 0, respectively. We denote these functions, shown in Fig. 3, by $f_+(y)$ and $f_-(y)$, respectively. A necessary condition for $f(y)$ to have three or more roots is that the maximum of f_+ be positive and the minimum of f_- be negative (satisfied in the example in Fig. 3). A sufficient condition is that the maximum of f_- be positive and the minimum of f_+ be negative (not satisfied in the example in Fig. 3).

If $b_{ie}b_{ei}=0$, $f(y)$ has at most three roots, as shown in Sec. II C.

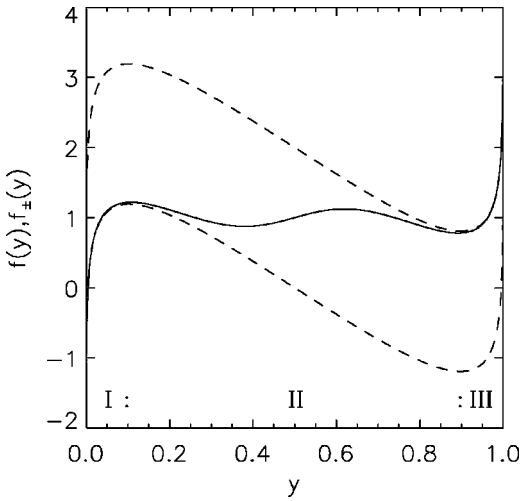

FIG. 3. Example of the behavior of the functions $f_+(y)$ (upper dashed curve) and $f_-(y)$ (lower dashed curve), defined in Sec. II E. The behavior of $f(y)$ in a case with one root is shown by the solid curve. Regions I, II, and III discussed in Sec. III A are labeled and their boundaries are indicated by colons.

3. Necessary conditions for five or more roots

For $f(y)$ to have five or more roots, all necessary conditions for three roots must be satisfied. In addition, $df(y)/dy$ must have a positive value at some point in zone II between the turning points of $f_\pm(y)$, as illustrated by the solid curve in Fig. 3. This curve also shows that this is not a *sufficient* condition.

III. PARAMETER DEPENDENCE OF STEADY STATES

When studying the dynamics of the cortex, stable steady states sit in basins of attraction for adiabatic dynamics, while unstable ones define the boundaries of these basins. (This is simply a consequence of the dynamics under the influence of relevant ''forces,'' a concept that is made more precise in Sec. IV.) Hence a key step in understanding cerebral dynamics systematically is to characterize the regimes of parameter space in which there are one, three, or five or more roots of the steady-state equation (17).

In this section we specialize to the particular form of sigmoidal function used in our previous work and in the illustrative figures in earlier sections [1,8–10,15,16]

$$\sigma(V_i)=\frac{1}{1+\exp[-C(V_i-V_0)]}, \tag{33}$$

where C and V_0 are constants. The inverse of σ is given by

$$\sigma^{-1}(y)=V_0+\frac{1}{C}[\ln y-\ln(1-y)]. \tag{34}$$

In the Appendix we show that this form of σ satisfies all the conditions assumed in Sec. II.

We wish to study the dependence of the number of roots on the parameters of our model, particularly the b_{mn} and V_0. We do this in a simplified way by restricting the interrelationships between the b_{mn} on physiological grounds. This reduces the dimensionality of parameter space, including

TABLE I. Classes of root structure of $f(y)$. The first column gives the category name, the numeral denoting the total number of roots (the minimum number in the 5^+ zone). The remaining three columns list the numbers of roots in zones I, II, and III of Fig. 3, respectively. Class $1A$ has no turning points of $f_{\pm}(y)$, so it is categorized separately since zones I–III are meaningless in this case.

Category	I	II	III
$1B$	1	0	0
$1C$	0	0	1
$1D$	0	1	0
$3A$	1	1	1
$3B$	0	2	1
$3C$	1	2	0
5^+	1	3	1

three dimensions corresponding to three independent b_{mn}. The root structure is then studied as a function of the b_{mn} for various values of the other parameters. The aim of this simplification is to obtain insight into a physiologically realistic class of dynamical models. In future work we aim to compare the dynamics of these models directly with experiment.

A. General topology of root structure

We want not only to distinguish the number of steady states of the cortex for specific parameters but to classify whether these are solutions corresponding to high Q_e (e.g., seizure states) or low Q_e (e.g., normal cortical states in which neurons fire at far less than their physiologically maximal values). We do this by counting the number of roots between and beyond the pair of turning points of $f_{\pm}(y)$ (zones labeled I, II, and III in Fig. 3), after separating off the case where $f_{\pm}(y)$ is monotonically increasing and these zones are undefined. This classification is crude in that the turning points are not fixed with respect to variations of the b_{mn}, but provides a useful coarse-grained categorization. This analysis also proves to be useful in constraining the types of adiabatic dynamics that are possible in the system. We will see in Sec. IV that $f(y)$ has dynamical significance beyond the positions of its roots: It is the gradient of an effective potential energy function in a physiologically realistic model of the cortex.

We label the case where $f_{-}(y)$ is monotonically increasing $1A$, where the number denotes the number of roots and the letter is an arbitrary label for the subcategory. The various other cases and their category labels are given in Table I, where they are distinguished by the numbers of roots in zones I, II, and III of Fig. 3. The possibilities listed (plus class $1A$) are exhaustive because the difference between $f(y)$ and $f_{-}(y)$ is monotonically increasing, which means that there can only be one or zero roots of $f(y)$ in either zone III or I, where $f_{-}(y)$ is also monotonically increasing. Figure 4 illustrates the appearance of $f(y)$ in each case.

As the underlying parameters of $f(y)$ (e.g., the b_{mn} and V_0) are changed, its roots appear or disappear in pairs. The only exceptions occur at sets of zero measure in parameter space where four roots can appear or disappear simultaneously or one pair can appear just as another disappears. Hence one-root and five-or-more-root zones of parameter space can touch at most at a set of measure zero. Similar arguments regarding $df(y)/dy$ imply that the $1A$ zone can touch the three-root zone at most at a set of measure zero. These and analogous arguments restrict the connectivities between zones to those shown in Fig. 5, which omits connections of zero measure. The key significance of this figure is that it constrains the paths that the system can take as its dynamics evolve under the influence of adiabatic feedbacks. For example, no robust (i.e., insensitive to slight changes in parameters) feedback mechanism can carry the system from the five-root zone to the one-root zone without passing through the three-root zone.

B. Random connectivity model of synaptic densities

In the simplest model for the development of interconnections between populations of inhibitory and excitatory neurons, the number of connections is proportional to the number of synapses available [8,16,17]. We term this the *random connectivity model,* but stress that other possibilities are also consistent with current physiological knowledge. Suppose excitatory neurons have fractions f_A and f_D, respectively, of the total numbers of axonal and dendritic synapses in the cortex, while inhibitory neurons have fractions $1-f_A$ and $1-f_D$. Suppose further that a fraction ϵ of all connections to cortical dendrites originate outside the cortex. Then, assuming random connectivities, the second column in Table II lists the fractions F_{mn} of connections from neuronal population n to population m, where the subscript s denotes subcortical origins. The third column lists the corresponding coefficients a_{mn} that appear in Eqs. (9) and (10). These are obtained from the F_{mn} via

$$a_{mn}=\frac{F_{mn}}{\sum_n F_{mn}}, \tag{35}$$

so that

$$\sum_m a_{mn}=1 \tag{36}$$

for all n. Equation (36) imposes a normalization that was neglected previously [1,8–10,15], but which is required to ensure that inputs to neurons are correctly weighted. (This did not make a large difference in these earlier works, which were primarily concerned with excitatory effects and had $\Sigma_n a_{en}\approx 0.9$.) This normalization applies to all models, not just the random connectivity model. One sees from Table II that $a_{en}=a_{in}$ for all n in the random connectivity model.

In earlier sections, the a_{mn} entered the cortical equations in the combination $b_{mn}=g_m a_{mn}$, where the g_m were synaptic gains. This model is too simple to study dynamical feedback, which can selectively affect the effective gain at synapses between particular populations of neurons rather than at all synapses at once. We thus generalize it by noting that every synaptic connection involves one neuron acting on another. A reasonable physiological approximation to the gain at a junction between an incoming neuron of population n and an outgoing one of population m is thus to factorize it

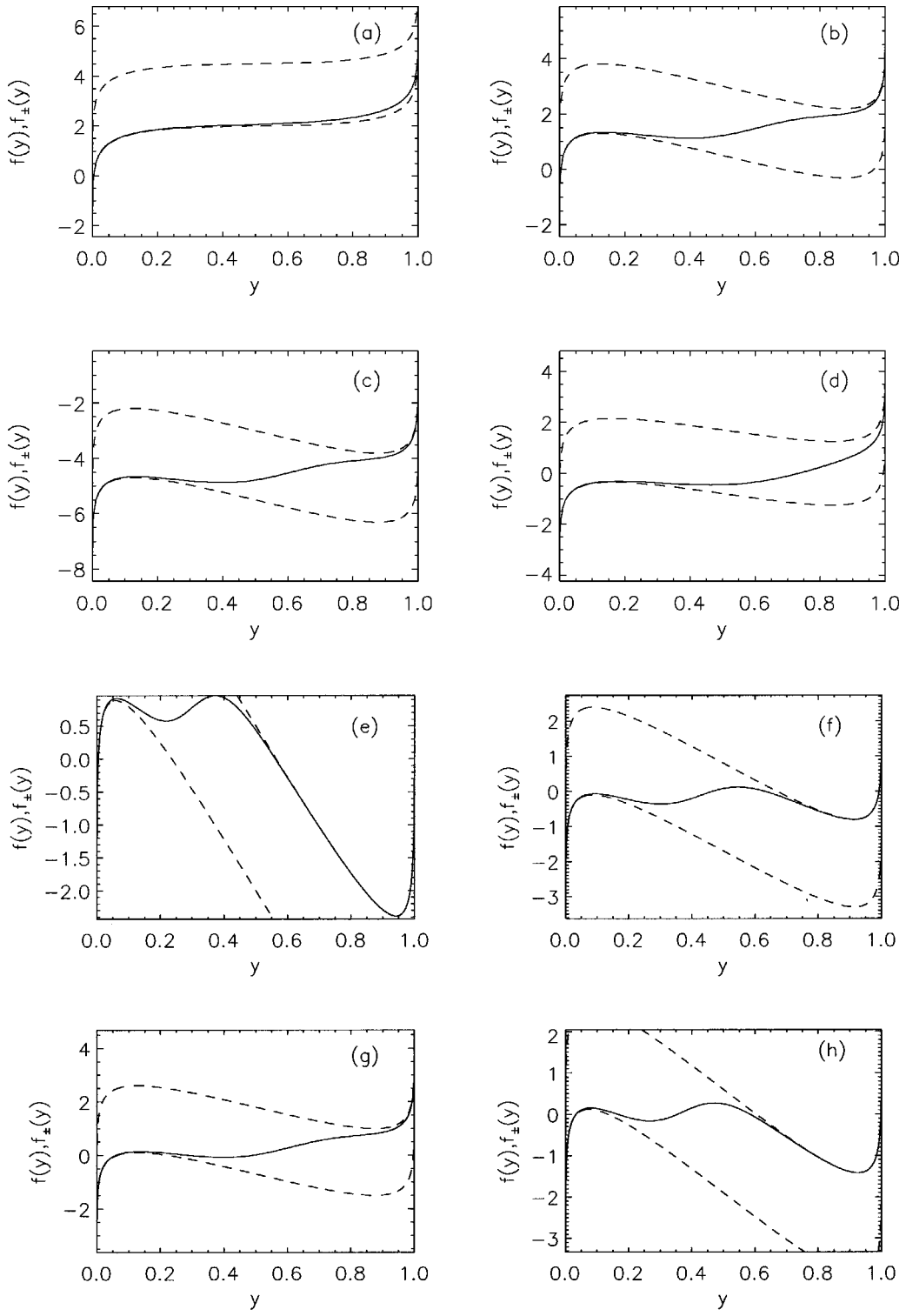

FIG. 4. Illustration of the seven root structures of $f(y)$ listed in Table I, plus the structure corresponding to class $1A$. Each case also shows $f_{\pm}(y)$ as dashed curves and is computed using Eqs. (33) and (34) with $b_{ei}=2.5$ and $b_{ii}=b_{is}=0$. Not all cases correspond to the random connectivity model of Sec. III B. (a) $1A$, with $b_{ee}=b_{ie}=2$ and $b_{es}=0$. (b) $1B$, with $b_{ee}=b_{ie}=5$ and $b_{es}=0$. (c) $1C$, with $b_{ee}=b_{ie}=5$ and $b_{es}=6$. (d) $1D$, with $b_{ee}=b_{ie}=4$ and $b_{es}=1.8$. (e) $3A$, with $b_{ee}=b_{ie}=10$ and $b_{es}=0$. (f) $3B$, with $b_{ee}=b_{ie}=6.2$ and $b_{es}=1.3$. (g) $3C$, with $b_{ee}=b_{ie}=5$ and $b_{es}=1.2$. (h) 5^{+}, with $b_{ee}=b_{ie}=8$ and $b_{es}=0.9$.

into the product of an absolute strength $|s_n|$ of the stimulus per unit incoming signal and a strength of response l_m per unit stimulus [16]. Physiologically, $|s_n|$ is proportional to the amount of chemical neurotransmitter released per unit incoming signal, while l_m measures the net response at the cell body per unit concentration of neurotransmitter at the synapses, including any effects of dendritic signal attenuation. The factors $|s_n|$ can be absorbed into the b_{mn} without loss of generality, but the l_m must then appear explicitly. (In general, the $|s_n|$ also incorporate different maximum firing rates for the various populations, which removes the need to normalize the sigmoidal functions to any value other than

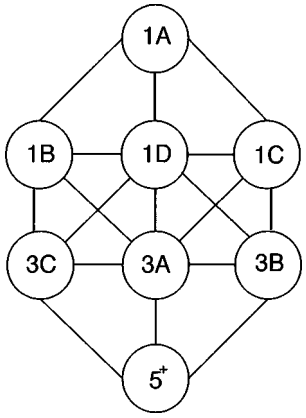

FIG. 5. Allowed connectivities between zones of parameter space corresponding to the eight classes of root structure. Zones can bound one another in parameter space at a set of nonzero measure only if they are linked by a line in this diagram.

unity.) This then leads to steady-state equations for this model of the same form as in previous sections, but with b_{mn} replaced by $l_m b_{mn}$ and

$$b_{in}=\frac{l_i}{l_e}b_{en} \tag{37}$$

for all n. Hence, for a fixed ratio l_i/l_e (only the ratio is an independent parameter), only three of the b_{mn} are independent in this model. This simplifies the study of its parameter space in what follows. Note that there is no analog of Eq. (36) for the b_{mn} once they have incorporated the $|s_n|$.

Previous works [1,8–10,15–17] have argued on physiological grounds that a_{ee} and a_{ie} (equal in the random connectivity model) are larger than the other a_{mn}. Although we do not impose such a restriction in the present work, we consider maximal values of $b_{ee}=b_{ie}$ that are larger than those of the other b_{mn} in the specific numerical examples discussed below.

C. Parameter dependence of root structure of the random connectivity model

We can now apply the conditions discussed in Sec. II E to study the occurrence of various numbers of roots in the random connectivity model with σ given by Eq. (33). We consider three regimes, depending on the size of the ratio l_i/l_e.

TABLE II. Fractional synaptic densities F_{mn} and the corresponding coefficients a_{mn} from Eqs. (9) and (10), calculated from the random connectivity model. Excitatory neurons have fractions f_A and f_D of cortical axonal and dendritic synapses, respectively, while extracortical connections occupy a fraction ϵ of the total cortical dendritic synapses.

mn	F_{mn}	a_{mn}
ee	$(1-\epsilon)f_A f_D$	$(1-\epsilon)f_A$
ei	$(1-\epsilon)(1-f_A)f_D$	$(1-\epsilon)(1-f_A)$
es	ϵf_D	ϵ
ie	$(1-\epsilon)f_A(1-f_D)$	$(1-\epsilon)f_A$
ii	$(1-\epsilon)(1-f_A)(1-f_D)$	$(1-\epsilon)(1-f_A)$
is	$\epsilon(1-f_D)$	ϵ

1. General l_i/l_e

A sufficient condition for exactly one root to occur is that $f(y)$ be monotonically increasing. This is certainly the case if $f_-(y)$ is monotonically increasing because $\sigma(V_i)$ in Eq. (17) is a monotonically increasing function of y (see Sec. II C). Using Eq. (A4), we thus find that zone $1A$ of parameter space satisfies

$$b_{ee}<4/C, \tag{38}$$

which is the condition for $f_-(y)$ to have no turning points. All three-root and five-root zones must satisfy the reverse inequality.

A further necessary condition for three roots to exist is that the maximum of f_+ be positive and the minimum of f_- be negative. Equations (17) and (A2) imply that the turning points of $f_\pm(y)$ occur at

$$y=\frac{1}{2}\left[1\pm\left(1-\frac{4}{Cb_{ee}}\right)^{1/2}\right]. \tag{39}$$

If $b_{ee}\gg 4/C$, one then has $y\approx 1/Cb_{ee}$, $1-1/Cb_{ee}$, with the maximum of $f_\pm$ occurring at the first of these two roots. Substitution of this approximate value of y into Eqs. (17) and (34) yields the following condition for f_+ to be positive:

$$b_{ee}<\frac{1}{C}\exp[CV_0-1+Cb_{ei}-Cb_{es}\phi_s]. \tag{40}$$

For the minimum of $f_-(y)$ to be negative, a similar analysis to the above but for $y\approx 1$ yields the requirement

$$b_{ee}>\frac{1}{C}\{u+\ln[u+\ln(u+\cdots)]\}, \tag{41}$$

$$u=CV_0-Cb_{es}\phi_s+1. \tag{42}$$

The upper bound (40) increases exponentially with V_0, whereas the lower bound (41) only increases linearly.

For five roots to occur, $f(y)$ must necessarily have a positive slope somewhere between the turning points of $f_\pm(y)$. The first two terms in the relevant expression (32) are negative in total between the turning points of $f_-(y)$, while the last peaks where σ' peaks, i.e., where $V_i=V_0$ and $\sigma'=C/4$ from the Appendix. Replacing the first term on the right-hand side of Eq. (32) by its minimum $4/C$ and the last term by its maximum value, a necessary condition for five or more roots to occur is found to be

$$(1+b_{ii}C/4)(b_{ee}-4/C)<Cb_{ei}b_{ie}/4. \tag{43}$$

On making the identification (37) for the random connectivity model, one finds that this requirement cannot be satisfied for $b_{ee}>4/C$ for any choice of l_i/l_e, so no five-or-more-root zone can exist.

2. $l_i/l_e\gg 1$

If $l_i/l_e\gg 1$ we can improve on the estimate (43). Specifically, Eqs. (14) and (37) imply that V_i increases with l_i.

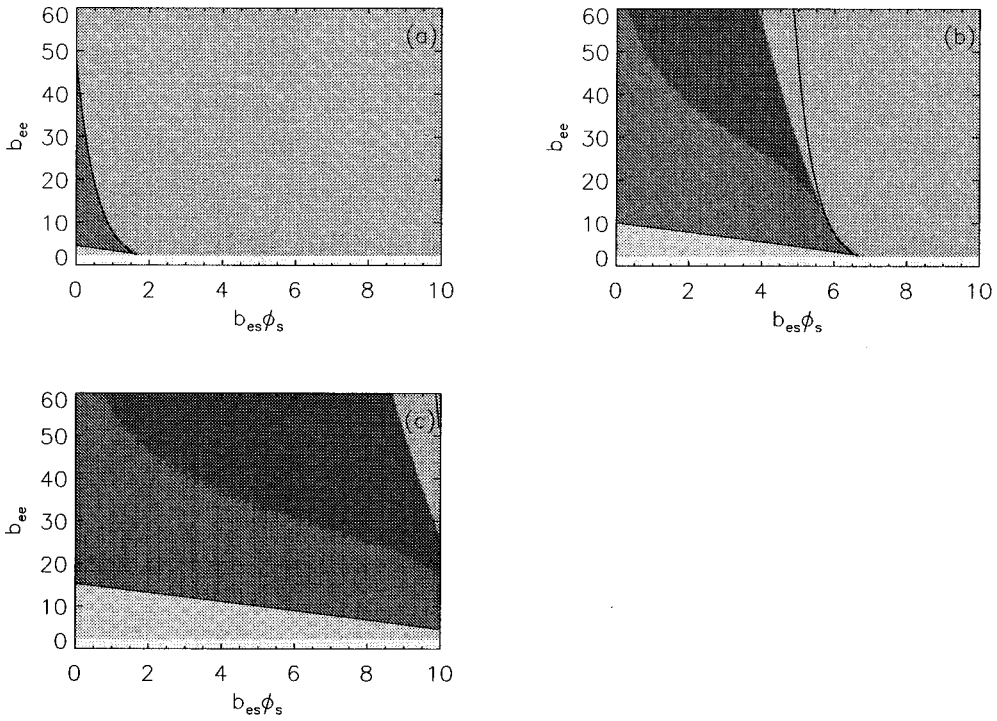

FIG. 6. Root structure as a function of parameter space for the random connectivity model with $V_0=3$, $C\approx 1.81$, and $l_i/l_e=4$. The zones from Table I are shown as functions of $b_{es}\phi_s$ and b_{ee} for various b_{ei}. In order of increasing darkness the zones are $1A$, $1B$, $1C$, $3A$, and $3B$. Small irregularities in the boundaries between zones are artifacts of the numerical calculations. The analytic bounds of the three-root zone, Eqs. (40) and (41) with Eq. (44), are shown for comparison as solid curves. (a) $b_{ei}=0$, (b) $b_{ei}=5$, and (c) $b_{ei}=10$.

Hence, for sufficiently large l_i, V_i exceeds V_0 and $f(y)\approx f_+(y)$ over most of the range in y, particularly at large y where f has a minimum. Similar arguments to those leading to Eq. (41) then imply that the three-root zone satisfies Eq. (41), but with

$$u=CV_0+1+Cb_{ei}-Cb_{es}\phi_s. \tag{44}$$

Figure 6 shows the one-root and three-root zones as functions of $b_{es}\phi_s$ and b_{ee} for three values of b_{ei}, $V_0=3$, and $l_i/l_e=4$. The conditions (40) and (41) with Eq. (44), shown for comparison, are seen to provide reasonable estimates of the boundaries of the three-root zone (although the upper bound errs significantly on the high side for large b_{ei}), while the boundary of zone $1A$ is consistent with Eq. (38). The connectivities between the various subzones are seen to accord with Fig. 5, although there are no zones of type $1D$ or $3C$ in this case. The case $b_{ei}=0$, shown in Fig. 6(a), corresponds to a purely excitatory network of cortical neurons. This case has been previously studied with equivalent results [1].

3. $l_i/l_e=1$

A number of simplifications follow if we specialize to the case $l_i/l_e=1$. Most importantly, Eqs. (13)–(15) imply $V_e=V_i=\sigma^{-1}(y)$. Hence we find

$$f(y)=\sigma^{-1}(y)-(b_{ee}-b_{ei})y-b_{es}\phi_s. \tag{45}$$

This function has the same functional form as $f_\pm(y)$ and hence can have only zero or two turning points and one or three roots. In this special case there are turning points only for $b_{ee}-b_{ei}>4/C$ and then the three-root zone satisfies the necessary and sufficient conditions $f(y)>0$ at the left turning point of f and $f(y)<0$ at the right turning point. If $b_{ee}-b_{ei}\gg 4/C$ these conditions become

$$b_{ee}-b_{ei}>\frac{1}{C}\{u+\ln[u+\ln(u+\cdots)]\}, \tag{46}$$

$$u=CV_0+1-Cb_{es}\phi_s, \tag{47}$$

$$b_{ee}-b_{ei}<\frac{1}{C}\exp[CV_0-1-Cb_{es}\phi_s]. \tag{48}$$

Equation (48) and the restriction $b_{ee}-b_{ei}>4/C$ immediately imply the condition

$$b_{es}\phi_s<(CV_0-1-\ln 4)/C \tag{49}$$

on the three-root zone and hence

$$V_0>(1+\ln 4)/C \tag{50}$$

for three roots to exist for positive $b_{es}\phi_s$.

Figure 7 shows the one-root and three-root zones as functions of $b_{es}\phi_s$ and b_{ee} for two values of b_{ei}, $V_0=3$, and $l_i/l_e=1$. The conditions (46) and (48), shown for comparison, are seen to provide very good estimates of the boundaries of the three-root zone, while Eq. (49) is also satisfied. As in Fig. 6, the connectivities between the various zones are in accord with Fig. 5.

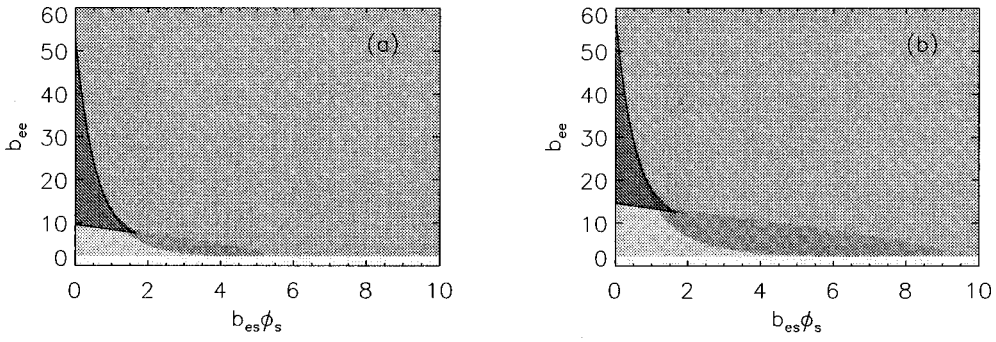

FIG. 7. Root structure as a function of parameter space for the random connectivity model with $V_0=3$, $C\approx 1.81$, and $l_i/l_e=1$. The zones from Table I are shown as functions of $b_{es}\phi_s$ and b_{ee} for various b_{ei}. In order of increasing darkness the zones are $1A$, $1B$, $1C$, $1D$, $3A$, and $3B$. Small irregularities in the boundaries between zones are artifacts of the numerical calculations. The analytic bounds of the three-root zone, Eqs. (46) and (48), are shown for comparison as solid curves. (a) $b_{ei}=5$ and (b) $b_{ei}=10$.

4. $l_i/l_e \ll 1$

In this case $V_i \ll V_0$ and inhibitory neurons thus have little effect on the cortical dynamics. The resulting root structure is very close to that of Fig. 6(a), with only a very weak dependence on b_{ei}.

IV. GLOBAL CORTICAL DYNAMICS OF THE RANDOM CONNECTIVITY MODEL

Many cortical phenomena occur on spatial scales comparable to the whole cortex and on time scales much longer than those of dendritic integration in individual neurons or even the faster cortical rhythms (a few tens of milliseconds). In particular, there are slow rhythms (so-called delta and theta rhythms) and so-called slow waves, which are prolonged deviations of cell potential without oscillatory components. These typically have time scales of 100 ms or longer [13], as do chemical feedback mechanisms that modulate the overall state of the cortex. Similarly, the evoked response potentials that follow a stimulus have time scales of several hundred milliseconds and are known to involve conditioning over even longer periods [13]. Previous theoretical work has also shown that the globally uniform ($k=0$) mode is the least stable or most unstable and hence it is likely to play a significant role in the dynamics [1].

In this section we use the results of the preceding analysis as the groundwork to treat large-scale cortical dynamics on long time scales. In the future, this treatment will form the basis of understanding adiabatic control of the cortical state via feedback or external stimuli. We specialize to the case of spatially uniform (global) dynamics on time scales much longer than those the dendritic integration time of ~ 10 ms. In Sec. IV A we derive the relevant equations of motion for the random connectivity model with $l_i/l_e=1$, which yields closed-form analytic results. Section IV B treats linear dispersion and stability, reproducing and generalizing previous results in the adiabatic regime. Numerical results in Sec. IV C illustrate these results by applying them to large-scale dynamics and to the cortical response to sinusoidal variations of ϕ_s.

A. Adiabatic global cortical dynamics

The equations of global cortical dynamics (GCD) are those of Sec. II A, with the deletion of the Laplacian term in Eq. (8). If we specialize to adiabatic dynamics with time scales much longer than the dendritic integration time constants α^{-1} and β^{-1}, Eqs. (5)–(7) are replaced by Eq. (11). For $l_i=l_e$ one also has $V_i=V_e$, $Q_i=Q_e$, and $Q_{ai}=Q_{ae}$.

We introduce the notation

$$D_{e,i}=\frac{1}{\gamma_{e,i}^2}\left(\frac{d^2}{dt^2}+2\gamma_{e,i}\frac{d}{dt}+\gamma_{e,i}^2\right). \tag{51}$$

Noting that γ_i is extremely large for typical cortical parameters [1], we can make the local inhibition approximation $D_i\approx 1$ [1], which yields $\phi_i=Q_i=Q_e$ via Eq. (8). Using Eq. (8) again we find

$$D_e\phi_e=Q_e \tag{52}$$

$$=\sigma(V_e) \tag{53}$$

$$=\sigma(gQ_{ae}) \tag{54}$$

$$=\sigma(b_{ee}\phi_e-b_{ei}Q_e+b_{es}\phi_s), \tag{55}$$

where Eqs. (1), (9), and (11) and the local inhibition approximation have been used in obtaining Eqs. (53) and (54). We have also written $b_{mn}=g_m a_{mn}$ in Eq. (55), as in previous sections, but now reinterpret the b_{mn} in the generalized way introduced in Sec. III B (i.e., the b_{mn} incorporate the stimulus strength $|s_n|$).

If we rewrite Eq. (55) using $y=Q_e=\sigma(V_e)$, as in previous sections, a comparison with Eq. (52) yields

$$\sigma^{-1}(y)=b_{ee}\phi_e-b_{ei}y+b_{es}\phi_s \tag{56}$$

and hence

$$D_e h(y)=b_{ee}y, \tag{57}$$

$$h(y)=\sigma^{-1}(y)+b_{ei}y-b_{es}\phi_s. \tag{58}$$

Equation (57) is equivalent to the motion of a Newtonian particle under the influence of both frictional and conservative forces, as can be seen by writing it in the form

$$\frac{d^2h(y)}{dt^2}=-2\gamma_e\frac{dh(y)}{dt}+\gamma_e^2[b_{ee}y-h(y)]. \tag{59}$$

The first and second terms on the right-hand side of Eq. (59) represent frictional and conservative forces, respectively. The fixed points of Eq. (59), representing the steady states of the system, coincide with the roots of the function $f(y)$ discussed in previous sections since $f(y)=h(y)-b_{ee}y$. The function $f(y)$ is thus proportional to the conservative part of the force, but has the opposite sign.

If friction dominates, accelerations are small and Eq. (59) can be simplified to

$$\frac{dy}{dt}\approx\frac{\gamma_e[b_{ee}y-h(y)]}{2\left[\dfrac{d\sigma^{-1}(y)}{dy}+b_{ei}\right]}. \tag{60}$$

Equation (60) has the same fixed points as Eq. (59) and its denominator is positive definite.

It is possible to formulate Eq. (59) in terms of a potential $U(h)$ via

$$U(h)=\gamma_e^2\int_{h_0}^{h}[h'-b_{ee}y(h')]dh', \tag{61}$$

where h_0 is an arbitrary reference point, which we place at $h_0=0$, and h' is a dummy variable. The inverse $y(h)$ exists and is unique because dh/dy is positive definite. Integration by parts yields

$$U(h)=\frac{\gamma_e^2}{2}\left[h^2-2b_{ee}\left(hy-\int_{y_0}^{y}h(y')dy'\right)\right], \tag{62}$$

where $y_0=y_0(h_0)$ and y' is a dummy variable. If we substitute the explicit form (34) for $\sigma^{-1}(y)$ into Eq. (58), we find

$$\begin{aligned}U(h)=\frac{\gamma_e^2}{2}\Bigg[h^2-2b_{ee}\Bigg\{&hy+(b_{es}\phi_s-V_0)(y-y_0)\\&-\frac{b_{ei}}{2}(y^2-y_0^2)-\frac{1}{C}[y\ln y-y_0\ln y_0\\&+(1-y)\ln(1-y)-(1-y_0)\ln(1-y_0)]\Bigg\}\Bigg],\end{aligned} \tag{63}$$

with

$$h(y)=V_0+\frac{1}{C}\ln\left(\frac{y}{1-y}\right). \tag{64}$$

It is worth noting that $U(h)$ in Eq. (63) is measured relative to a point h_0 that depends on the b_{mn}. Since the zero of U is arbitrary, one can always reexpress it relative to a point that does not depend on the b_{mn} or V_0. Specifically, if one chooses this point to be the unique point where $h_0=0$ when all the b_{mn} are zero and $V_0=0$, one must use $y_0=1/2$ in Eq. (63).

Figure 8 shows an example of $U(h)$, plotted against y, in zone $3A$ of Fig. 6(a), near the boundary with zone $1B$. Note the two minimums, corresponding to the stable fixed points, and one maximum at the unstable fixed point. The divergences of $U(h)$ as $y\to 0,1$ prevent the system from reaching these points. As the boundary of zone $1B$ is approached and crossed, the right-hand minimum potential rises to exceed the potential at the maximum, leaving only the left-hand minimum. Likewise, the boundary of zone $1C$ corresponds to the central maximum falling below the left-hand minimum, leaving only the right-hand minimum.

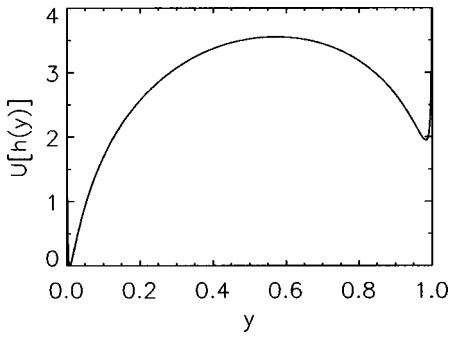

FIG. 8. Potential $U(h)$ vs y, given by Eq. (67) for the random connectivity model with $b_{ee}=5$, $b_{ei}=0$, and $b_{es}\phi_s=0.3$, near the boundary between zones $3A$ and $1B$ in Fig. 6(a).

Formulation of GCD in terms of a potential emphasizes the physical requirement that fixed points of the system must alternate between stable and unstable in character [apart from degenerate cases of multiple coincident roots of $f(y)$]: Between any two minimums of $U(h)$ there must be a maximum. Moreover, the first and last fixed points must be stable or else the system would have additional fixed points at infinite $V_{e,i}$, which is a contradiction. These conclusions are not restricted to the random connectivity model with $l_i=l_e$, but hold for general forms of σ and arbitrary coefficients b_{mn} for the same physical reasons.

B. Linear dispersion and stability

In the case of small perturbations from a fixed point y_f, Eq. (57) can be Fourier transformed to yield the linear dispersion equation

$$(\gamma_e-i\omega)^2=\frac{\gamma_e^2 b_{ee}}{\dfrac{d\sigma^{-1}(y_f)}{dy}+b_{ei}}, \tag{65}$$

where the notation in Eq. (65) indicates that the derivative of $\sigma^{-1}(y)$ is to be evaluated at y_f. This result reproduces Eq. (55) of Ref. [1] for zero wave number ($k=0$), $l_i=l_e$, and $b_{ei}=0$, although this earlier result was in a somewhat different notation.

The instability threshold of a fixed point can be calculated from the point where the imaginary part of ω is zero [1]. Hence we find that instability occurs for

$$b_{ee}>\frac{d\sigma^{-1}(y_f)}{dy}+b_{ei}. \tag{66}$$

This result generalizes Eq. (57) of Ref. [1] to nonzero b_{ei} for $l_i=l_e$ and $k=0$. It confirms physical intuition in that feedback from the inhibitory neurons to the excitatory ones raises the instability threshold.

Sufficiently strong in-phase feedback of a subject's EEG (by allowing it to modulate a flickering light source in their field of vision, for example) will rapidly induce a seizure [18], as will chance correlations of external flicker with EEG

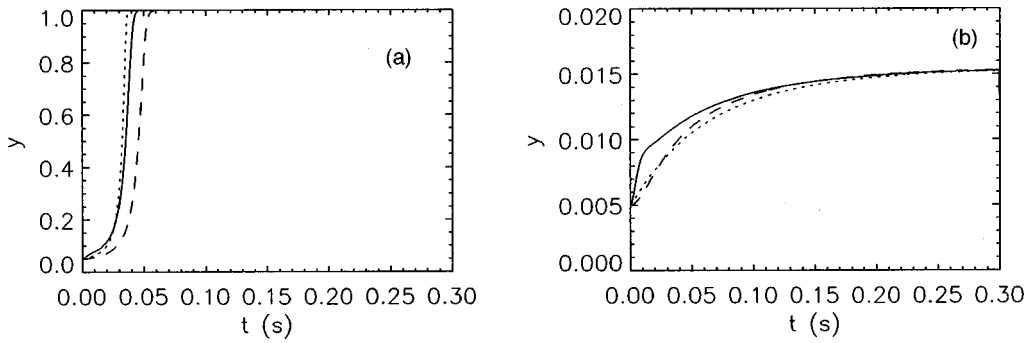

FIG. 9. Comparison of the dynamics for the full and adiabatic GCD equations for a random connectivity model system with $b_{ee}=30$, $b_{ei}=3$, and $b_{es}\phi_s=0.3$. The solid line shows the full result for $\alpha=\beta=400\ \mathrm{s}^{-1}$, while the dotted and dashed lines show results from the first-order approximation (60) and the second-order approximation (59), respectively. (a) System initialized with $y=0.05$. (b) System initialized with $y=0.005$.

signals [18,19], so-called *photic* epilepsy. This implies that the instability threshold (66) has been lowered. We can estimate the threshold for such feedback-induced seizures by replacing ϕ_s in Eq. (58) by $Ae^{i\psi}(y-y_f)$, where A and ψ are real constants representing the amplitude and phase of the feedback signal. After linearizing the resulting equation, we find a dispersion equation of the form (65) with the replacement

$$b_{ei}\rightarrow b_{ei}-b_{es}Ae^{i\psi}. \tag{67}$$

Instability occurs for

$$b_{ee}>\frac{d\sigma^{-1}(y_f)}{dy}+b_{ei}-b_{es}A\ \cos\psi, \tag{68}$$

where the minimum threshold occurs at $\omega=0$. The threshold is lowered relative to Eq. (66) for in-phase feedback and raised for feedback that is π out of phase. As one might expect, the effect of feedback that is π out of phase is equivalent to increasing b_{ei}, the coefficient that describes the effect of inhibitory neurons on excitatory ones. Seizure induction, as well as the variation of its threshold with ψ, provides a potential experimental test of the theory presented here and in previous works [1,16].

C. Nonlinear dynamics and the effects of dendritic integration

Figure 9 compares solutions of the full GCD equations including the effects of dendritic integration for realistic physiological values $\alpha=\beta=400\ \mathrm{s}^{-1}$ in Eqs. (5)–(7), with the first- and second-order adiabatic approximations (60) and (59). The parameters correspond to a point in zone $3A$ with two stable fixed points separated by one unstable one. In this case, Eqs. (5)–(7), (9), and (10) are replaced by

$$\left(\frac{d^2}{dt^2}+2\alpha\frac{d}{dt}+\alpha^2\right)V_{e,i}=\alpha^2[(b_{ee}-b_{ei})\phi_e-b_{es}\phi_s] \tag{69}$$

for $l_i=l_e$. Figure 9(a) shows a case where the system is initialized in the basin of attraction of the highest fixed point, which corresponds to a seizure state, but near the middle (unstable) fixed point. The full GCD equations and Eqs. (59) and (60) all imply that the system accelerates to larger y, before approaching the highest fixed point asymptotically with t. The full solution, including dendritic effects, has an initial steep transient, followed by very similar behavior to the other solutions. The time evolution is very similar apart from a few milliseconds lag between the curves. Figure 9(b) shows results for the same system as in Fig. 9(a), except that it was initialized below the lowest fixed point. In this case, the three solutions are again similar after a $\sim$10-ms transient in the full solution, converging smoothly toward the fixed point. Neither Eq. (59) nor Eq. (60) shows clear superiority over the other in this case.

The adiabatic approximation made in deriving Eqs. (59) and (60) depends on α $(=\beta)$ being larger than the inverse time scale of the global dynamics. Figure 10 shows the effect of varying α over the range $1000-100\ \mathrm{s}^{-1}$. In each case the system is the same as in Fig. 9, except that it is initialized slightly above the lowest fixed point. For $\alpha>200\ \mathrm{s}^{-1}$, Eqs. (59) and (60) give reasonable approximations to the dynamics in this and other examples investigated, in accord with physical expectations. Again, neither approximation can be strongly preferred on the grounds of accuracy.

Figure 11 shows a further comparison of the full GCD equations with the approximations (59) and (60). In these results, a 10% sinusoidal modulation of ϕ_s was superposed on a mean value of unity. The figure shows that Eqs. (59) and (60) give good approximations to the actual behavior for frequencies below about 10 Hz, consistent with the results in Figs. 9 and 10. At higher frequencies, the first-order result (60) greatly underestimates the amplitude of the oscillations relative to the full result, indicating that high frequencies are more strongly damped in the corresponding adiabatic dispersion equation than in the full one. The second-order result (59) gives a good approximation to the dynamics for frequencies $\lesssim$30 Hz, with an upper bound to its regime of validity of 10–20 Hz for $\alpha=100\ \mathrm{s}^{-1}$. This upper bound is not a significant limitation since the adiabatic approximation is not intended to be valid at frequencies above about 10 Hz in any case and only applies for $\alpha\gtrsim 100\ \mathrm{s}^{-1}$.

V. SUMMARY

In this work we have investigated the steady states and global dynamics of our recent continuum model of electrical activity in the cerebral cortex, generalized to allow for different effective gains at synapses between different populations of neurons. Particular attention has been paid to the

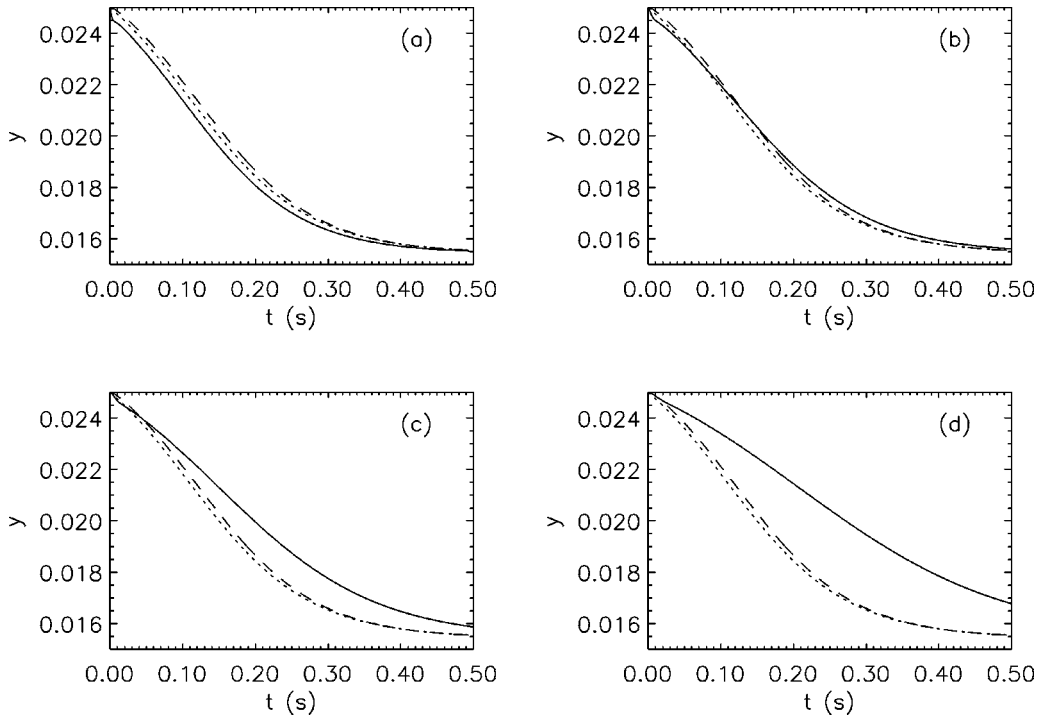

FIG. 10. Effect of α $(=\beta)$ on the agreement between the full and adiabatic GCD equations for the same system as in Fig. 9, but initialized with $y=0.025$. The solid line shows the full result, while the dotted and dashed lines show results from the first-order approximation (60) and the second-order approximation (59), respectively. (a) $\alpha=1000\ \mathrm{s}^{-1}$. (b) $\alpha=400\ \mathrm{s}^{-1}$. (c) $\alpha=200\ \mathrm{s}^{-1}$. (d) $\alpha=100\ \mathrm{s}^{-1}$.

steady states of the system and to adiabatic global dynamics.

General criteria for the occurrence of various numbers of cortical steady states have been found. In the case of our previously used sigmoidal function (33), a maximum of three roots can occur for the random connectivity model (other models can have at least five, although we have not yet found any cases with more than five, despite searching extensively). The regions of parameter space in which various numbers of roots occur have been studied for this model and their boundaries have been found to be consistent with the

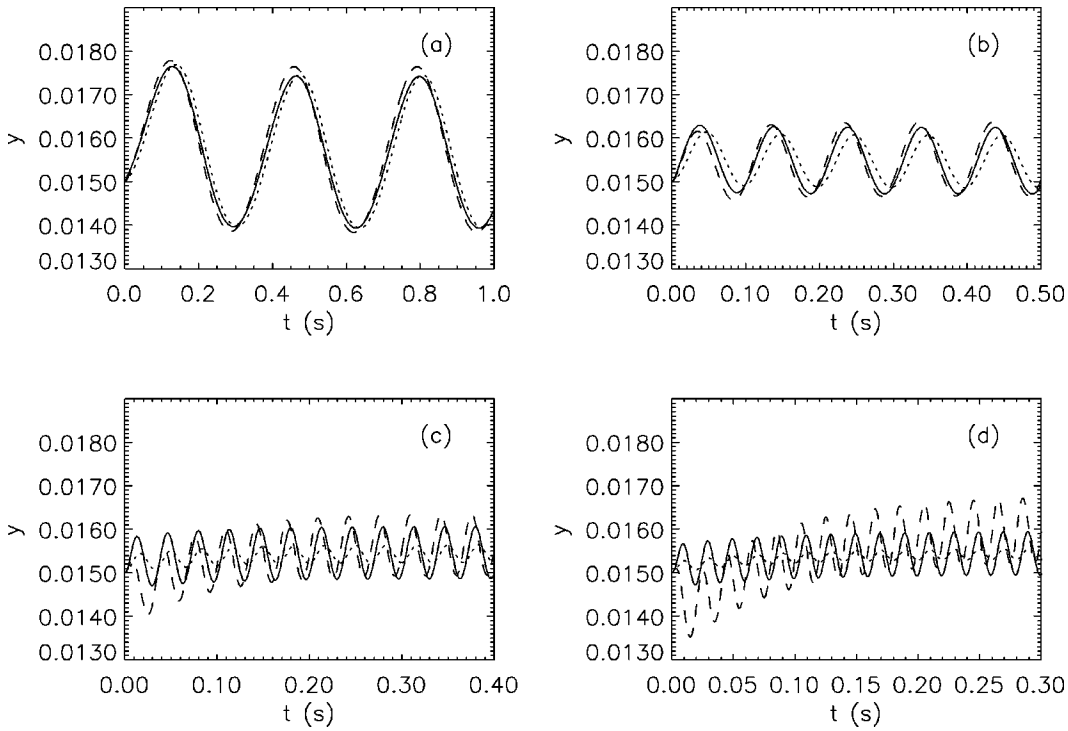

FIG. 11. Comparison of the full and adiabatic frequency responses of the same system as in Figs. 9 and 10, where a 10% sinusoidal modulation has been added to ϕ_s. The solid line shows the full result, while the dotted and dashed lines show results from the first-order approximation (60) and the second-order approximation (59), respectively. (a) Modulation at 3 Hz. (b) Modulation at 10 Hz. (c) Modulation at 30 Hz. (d) Modulation at 50 Hz.

analytic criteria obtained here.

For a particular case of our model, in which the characteristic response strengths of excitatory and inhibitory neurons are equal ($l_i = l_e$), Eqs. (59) and (60) have been obtained as approximations to the full GCD equations (1), (5)–(10), and (33) with ∇^2 replaced by zero in Eq. (8). Equation (59), a second-order equation, is equivalent to the equation of motion of a Newtonian particle in a potential in the presence of friction. Equation (60) applies in the case that friction dominates the dynamics. We have obtained explicit forms for the potential and force functions, allowing us to characterize the basins of attraction of the steady states.

The approximate linear dispersion relation (65) generalizes the results of previous work [1] to include inhibitory effects more fully in the adiabatic limit for $k=0$. Stability boundaries are also generalized to include the effects of inhibition and direct feedback of cortical signals as input. The results confirm that inhibition raises the instability threshold, while feedback can either raise or lower it depending on its phase relative to the signal.

Numerical results have confirmed that the adiabatic GCD equations approximate the full ones adequately for dendritic integration times in the physiologically observed range, provided the characteristic time scales of the dynamics are longer than about 100 ms. The response to sinusoidal modulations of the system is also found to agree well for frequencies below about 10 Hz.

The results obtained here provide the basis from which to address the effects of feedback on large-scale cortical dynamics in future work. Steady states are the most fundamental features of the dynamical system. Their basins of attraction can evolve as a result of the feedback mechanisms that are known physiologically to operate on the cortex, thereby allowing for more complicated dynamics, possibly including limit cycles or chaotic evolution (which may, of course, also occur on faster time scales as a result of voltage-dependent changes in ionic conductivities of neuronal membranes, for example). Many features of EEGs are large scale and occur in the adiabatic temporal regime. These include evoked response potentials, the alpha, delta, and theta rhythms [13], the characteristic ''spike and wave'' signal of petit mal seizures [13], and the progression of grand mal seizures [13]. The present work thus promises to have wide application in interpreting phenomena such as these and in determining the relevance of our model to such situations. Even when feedbacks and dynamics are not adiabatic, they occur against the background of the instantaneous fixed points and their basins of attraction that still constrain the dynamics. One further effect that must be incorporated is the existence of spatially nonuniform eigenmodes and the resulting nonlinear mode-mode interactions. Such interactions are likely to be just as important as feedbacks and must be included simultaneously in any attempt to obtain a detailed understanding of cortical waves and EEGs. Nonetheless, spatially uniform modes include the least damped cortical responses and are thus likely to contain the largest spectral response to complex or noisy cortical inputs.

ACKNOWLEDGMENTS

The authors thank M. Roy for preparing Fig. 5. This work was supported by the Ross Trust, Melbourne, and the Australian Research Council.

APPENDIX: VERIFICATION THAT THE REQUISITE CRITERIA ARE SATISFIED BY THE SPECIFIC FORM (33) OF σ

In this appendix we verify that the form of σ used in our previous work has all the properties required in Sec. II. The sigmoidal function we have used and its inverse are given by Eqs. (33) and (34). We find the following results by repeated differentiation of these expressions:

$$\frac{d\sigma(V_i)}{dV_i} = C\sigma(1-\sigma), \tag{A1}$$

$$\frac{d^2\sigma(V_i)}{dV_i^2} = C^2\sigma(1-\sigma)(1-2\sigma), \tag{A2}$$

$$\frac{d^3\sigma(V_i)}{dV_i^3} = C^3\sigma(1-\sigma)(1-6\sigma+6\sigma^2), \tag{A3}$$

$$\frac{d\sigma^{-1}(y)}{dy} = \frac{1}{C}\left(\frac{1}{1-y}+\frac{1}{y}\right), \tag{A4}$$

$$\frac{d^2\sigma^{-1}(y)}{dy^2} = \frac{1}{C}\left(\frac{1}{(1-y)^2}-\frac{1}{y^2}\right), \tag{A5}$$

$$\frac{d^3\sigma^{-1}(y)}{dy^3} = \frac{2}{C}\left(\frac{1}{(1-y)^3}+\frac{1}{y^3}\right). \tag{A6}$$

The above expressions satisfy our requirements (2)–(4) in Sec. II A. It is straightforward to show that the expression in Eq. (A1) is non-negative and has a single peak, about which it is symmetric. All the derivatives shown are well defined and continuous in the relevant ranges. The maximum of Eq. (A1) is of order unity for C of order unity and $0<\sigma<1$.

We now turn to the additional criteria in Sec. II C. We find that Eq. (A4) is indeed symmetric about $y=1/2$ and that Eqs. (26)–(28) are satisfied.

[1] P. A. Robinson, C. J. Rennie, and J. J. Wright, Phys. Rev. E **56**, 826 (1997).

[2] F. H. Lopes da Silva, A. Hoeks, A. Smits, and L. H. Zetterberg, Kybernetik **15**, 27 (1974).

[3] A. van Rotterdam, F. H. Lopes da Silva, J. van den Ende, M. A. Viergever, and A. J. Hermans, Bull. Math. Biol. **44**, 283 (1982).

[4] W. J. Freeman, *Mass Action in the Nervous System* (Academic, New York, 1975).

[5] W. J. Freeman, in *Induced Rhythms of the Brain*, edited by E.

Başar and T.A. Bullock (Birkhauser, Basel, 1991).
[6] P. L. Nunez, IEEE Trans. Biomed. Eng. **BME-21**, 473 (1974).
[7] P. L. Nunez, in *Neocortical Dynamics and Human EEG Rhythms*, edited by P. L. Nunez (Oxford University Press, Oxford, 1995).
[8] J. J. Wright and D. T. J. Liley, Network **5**, 191 (1994).
[9] J. J. Wright and D. T. J. Liley, Biol. Cybern. **72**, 347 (1995).
[10] J. J. Wright and D. T. J. Liley, Behav. Brain Sci. **19**, 285 (1996).
[11] V. K. Jirsa and H. Haken, Phys. Rev. Lett. **77**, 960 (1996).
[12] V. K. Jirsa and H. Haken, Physica D **99**, 503 (1997).
[13] M. R. Rosenzweig and A.L. Leiman, *Physiological Psychology* (Random House, New York, 1989).
[14] I. Segev, in *Handbook of Brain Theory and Neural Networks*, edited by M. A. Arbib (MIT Press, Cambridge, MA, 1995).
[15] P. A. Robinson, J. J. Wright, and C. J. Rennie, Phys. Rev. E **57**, 4578 (1998).
[16] C. J. Rennie, P. A. Robinson, and J. J. Wright (unpublished).
[17] D. T. J. Liley and J. J. Wright, Network **5**, 175 (1994).
[18] W. G. Walter, *The Living Brain* (Duckworth, London, 1953).
[19] G. H. Glaser, in *Cecil Loeb's Textbook of Medicine*, edited by P.B. Beeson and W. McDermott (Saunders, Philadelphia, 1967).